Original Article

www.jmss.mui.ac.ir

Shape Adaptive, Robust Iris Feature Extraction from Noisy Iris Images

Hamed Ghodrati, Mohammad Javad Dehghani, Habibolah Danyali

Department of Telecommunication Engineering, Shiraz University of Technology, Shiraz, Iran

Submission: 19-01-2013 Accepted: 10-08-2013

ABSTRACT

In the current iris recognition systems, noise removing step is only used to detect noisy parts of the iris region and features extracted from there will be excluded in matching step. Whereas depending on the filter structure used in feature extraction, the noisy parts may influence relevant features. To the best of our knowledge, the effect of noise factors on feature extraction has not been considered in the previous works. This paper investigates the effect of shape adaptive wavelet transform and shape adaptive Gabor-wavelet for feature extraction on the iris recognition performance. In addition, an effective noise-removing approach is proposed in this paper. The contribution is to detect eyelashes and reflections by calculating appropriate thresholds by a procedure called statistical decision making. The eyelids are segmented by parabolic Hough transform in normalized iris image to decrease computational burden through omitting rotation term. The iris is localized by an accurate and fast algorithm based on coarse-to-fine strategy. The principle of mask code generation is to assign the noisy bits in an iris code in order to exclude them in matching step is presented in details. An experimental result shows that by using the shape adaptive Gabor-wavelet technique there is an improvement on the accuracy of recognition rate.

Key words: *Feature extraction, iris recognition, noise-removing, shape adaptive Gabor-wavelet, shape adaptive wavelet transform, statistical decision making*

INTRODUCTION

Since the last decade, tendency to replace traditional human identification systems with biometrics have been increased. Iris recognition is one of the accurate and reliable systems among the biometric traits. Recently, the endeavor is to relax the constraints on the iris acquisition to support user-friendly and surveillance applications. In this way, captured iris images contain various noise factors such as bad focus, motion blur, head tilt, eyelid and eyelash occlusions and reflections, out of framework, glasses and contact lenses. These artifacts lead to increase the false reject rate (FRR). Therefore, the noisy regions should be distinguished before feature extraction in a pre-processing stage called segmentation. The segmentation step is carried out in two sub-steps: Localization and noise-removing. The localization determines the borders of the iris while noise-removing involves in eliminating the noisy parts from localized region. Nevertheless, some scholars prefer to remove the noises after normalization step. The normalization is a scale invariant transform from Cartesian to polar coordinates. Daugman's rubber sheet model[1] is the most popular technique to normalize the iris region to a fixed rectangular image. One of the aspects of this research is to provide an effective noise-removing approach. The most probable noise factors are shown in Figure 1 using some localized and normalized iris images. In what follows describes these noise factors.

Eyelids

Natural position of eyelids is toobstruct some portions of the iris. Usually, intensity of eyelid areas is higher than the iris. Label 1 in Figure 1 illustrates the eyelid areas as noise factor.

Eyelashes

Eyelashes are distributed disorderly on the iris region, especially on the upper part. The intensity of eyelashes differs even in one iris image and it can change along each eyelash. Unfortunately, the gray level of some eyelashes is close to some iris patterns so that detecting them is difficult. Label 2 in Figure 1 shows some occluded regions by eyelashes.

Strong Reflections

This artifact arises from reflection of light source in front of the user. The noisy areas have intensity value close to maximum. Strong reflections are labeled by number 3 in Figure 1.

Address for correspondence:
Mr. Hamed Ghodrati, Department of Telecommunication Engineering, Shiraz University of Technology, Shiraz, Iran. E-mail: h.ghodrati@hotmail

Weak Reflections

This kind of reflections appears on account of the mirror-like operation of iris. Disruption of the iris patterns by weak reflections is less than the strong reflections. However, the environmental conditions caused the intensity value of these reflections would not be specific that it makes difficult to detect them. Label 4 is considered for them in Figure 1.

Out of Framework

In less cooperative systems, it is possible the captured image does not contain the iris region either partially or entirely. In the case of partial occlusion, the outer boundary would not be a complete circle and when the localized region is normalized to a rectangular block, the lost pixels are detected and replaced with maximum intensity value. Label 5 illustrates this noise factor in Figure 1.

Pupil and Sclera

In general, the iris boundaries are not actual circle.[2] Besides, because of localization error, it may be considered some portions of the pupil or the sclera as iris region. Bad segmented pupil and sclera can obstruct some upper and lower rows of normalized image, respectively. In Figure 1 Labels 6 and 7 are considered for the pupil and the sclera occlusions, respectively.

Our aim is to detect the noisy regions in the iris plane and generating a binary mask where the noisy pixels are separated from noise-free pixels. In many proposals, the noise mask have been obtained and used to exclude the noisy features in matching step. However, in the feature extraction step noisy information may affect the relevant features. In other words, if filters and transforms, which are used to extract the features, are applied to the segments of signal including both noisy and noise-free pixels, the extracted features in this way will be contaminated by corrupted data. Therefore, it is necessary to use the information of noise mask in the feature extraction step as well. We have not found any documentation in the literature to address this issue. Only Masek[3] replaced corrupted pixels by eyelashes with the intensity of intact nearest neighbor in pertaining row. The task of this paper is to study the effects of all noise factors on the noise-free features.

The reminder of this paper is structured as follows. Section 2 reports a literature review of noise-removing approaches. The localization and noise-removing method have been proposed in Section 3 and 4, respectively. Section 5 presents the shape adaptive iris feature extraction based on wavelet transform and Gabor-wavelet. Our experimental results are evaluated in Section 6. Finally, conclusions are offered in the last section.

LITERATURE REVIEW OF NOISE-REMOVING

In order to avoid the noise-removing step, some authors[4-6] proposed using of some portions of the iris where are less occluded by artifacts. Although this strategy reduces processing time, the recognition accuracy is reduced especially for large scale due to using partial discriminant

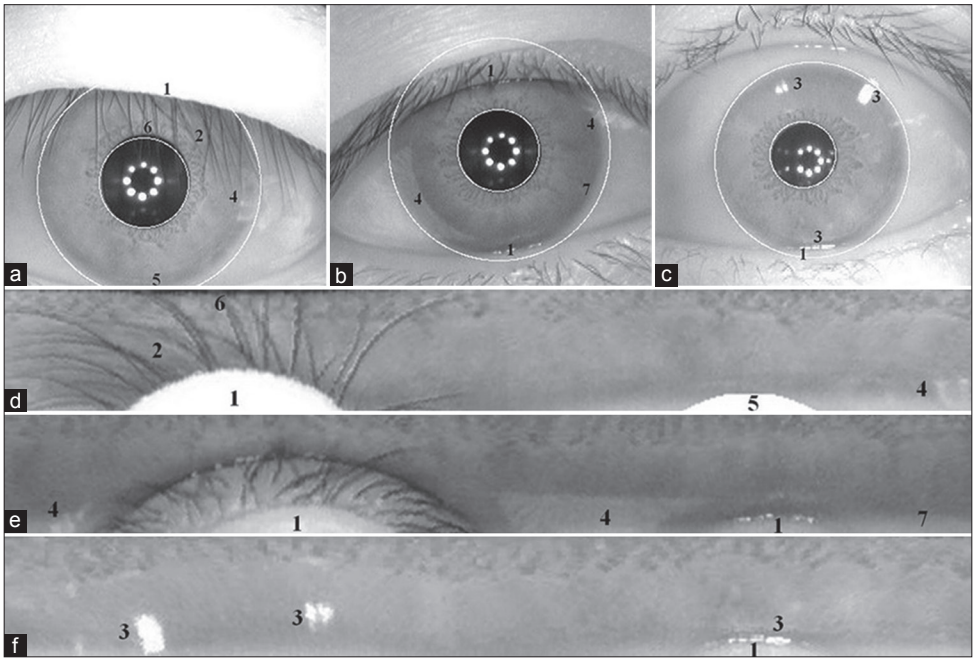

Figure 1: Noise factors: 1-eyelid, 2-eyelash, 3-strong reflection, 4-weak reflection, 5-out of framework, 6-pupil, 7-sclera. (a-c) Localized images, (d-f) Normalized images

information. Daugman[1] fitted the eyelids by changing the search model of integro-differential operator from circular to arcuate. He detected the eyelashes using thresholding.[2] The appropriate threshold was obtained based on the differences between intensity distributions of different iris regions. Masek[3] separated the eyelids from the localized iris region using the horizontal lines and detected the eyelashes by a constant threshold. In[7,8] authors used two and three lines to extract the eyelid model. Despite the linear approximations of the eyelids are higher computational efficiency, these methods are not accurate owing to the fact that the eyelids have a semi-parabolic shape. Hence, Kong and Zhang[9] detected the eyelids using parabolic Hough transform. They employed 1D Gabor filter as an edge detector to distinguish the separable eyelashes. Multiple eyelashes were segmented through measuring the standard deviation within small areas of the image. They specified the strong reflections by a constant threshold while the weak reflections were supposed the transitions from strong reflections to the iris region and detected them via an iterative algorithm around the strong reflections. However, it is seen in Figure 1 that the weak reflections are not always placed near the strong reflections. The eyelids detection efficiency is degraded by eyelash occlusion especially on the upper half of the iris region. Tan *et al*.,[10] to overcome this challenge, extracted the edges along the vertical direction from filtered image by use of 1D rank filter in the horizontal direction. Then the edges refinement is carried out through eliminating the noisy edge points that have less similarity to the learned eyelid curvature models. The eyelids were detected by fitting a parabola based on the refined edges. The eyelashes and shadows were identified by a proper threshold, which was obtained by a strategy similar to Daugman in.[2] They presented a smart prediction model that takes χ^2 distance between histogram of noisy and noise-free regions as input and calculated the occlusion percentage to get an appropriate threshold. Jang *et al*.[11] determined the eyelids searching the area by finding cross points between eyelids and the outer boundary. Then eyelid candidate points were obtained by some masks, which were designed based on the image focus. Finally, the eyelids were accurately segmented through adding rotation term into parabolic Hough transform. Their method to detect the eyelashes was based on selecting the thresholds and parameters values using focus assessment.[12] Min and Park[13] used the parabolic Hough transform for normalized iris image in place of the original image. The eyelashes were isolated by Otsu thresholding[14] on the feature image, which combined the intensity and local standard deviation values.

In spite of many accomplished studies, some issues have not yet been addressed. Firstly, the distorted areas by reflections have not been excluded or have been detected using a constant threshold while the reflections intensity changes from one image to another (especially weak reflections). Secondly, some algorithms such as Hough transform and Otsu thresholding can find the fittest solution, whereas it may not be the best from view of the system. This problem can deteriorate once the iris would not be occluded by eyelids or eyelashes. For instance, the authors of[13] applied Otsu thresholding whether the iris is obstructed or not by eyelashes. As a result, obtained threshold is not suitable as engenders some iris patterns are considered as eyelashes. Thirdly, some scholars used a part of iris images of database for training mode to get the appropriate threshold. This takes time to analysis the images and learning the model. Moreover, existence of the pupil or sclera in localized iris region due to inaccurate iris localization has not considered in most previous works. The Section 4 presents a novel method to remove the introduced noise factors in the first section and deal with all above shortcomings.

IRIS LOCALIZATION

The iris region could be localized by two circles as inner (pupil/iris) and outer (iris/sclera) boundaries. Iris localization must be fast and accurate. Hough transform is an effective tool to find various shapes in an image such as lines, circles and parabolas. Exploiting circular Hough transform due to searching in whole iris image is time-consumer. Specular reflections are bright regions on pupil, which are formed because of passing light through the cornea. The searching area of Hough transform can be confined through finding the location of specular reflections to reduce the computational burden. Hole-filling, a morphological operator fills dark holes surrounded by lighter region in the grayscale images. We apply this operator to the iris image to remove the specular reflections. Figure 2a and b show an iris image before and after removing of the specular reflections, respectively. Regarding that the pixels, in which difference

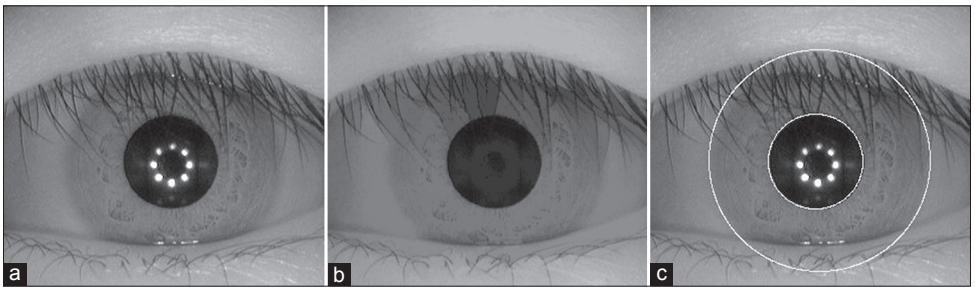

Figure 2: Iris localization. (a) Original iris image, (b) Removed specular reflections, (c) Localized iris image

between the original image and removed specular reflection image is high belong to pupil region, it constitutes a coarse estimation of pupil location. To accelerate in finding inner boundary, the circular Hough transform is applied for the edges near this estimation of pupil. Similarly, the outer boundary can be detected using circular Hough transform for center candidates close to the pupil center. To more speed up in finding the iris boundaries, the circular Hough transform is applied to low-resolution iris image. The shrink rate for inner and outer boundaries is not necessarily equal. Canny and Sobel edge detectors are used to extract the edges for detection of inner and outer boundary, respectively. Canny edge detector extracts thinner edges because of its non-maximum suppression procedure. It is suitable to extract the edges for inner boundary detection while it may jeopardize the task of effective outer boundary detection due to weak contrast between the iris and sclera comparing to pupil. The Sobel edge detector is applied only in the horizontal direction to decrease the effects of the eyelids on extracted edges. Figure 2c shows detected iris boundaries.

NOISE-REMOVING

The segmentation of the other noise factors, which likely obstruct the localized iris region is presented in this section. We apply this sub-step after normalization for two reasons: Neither considering the rotation factor in eyelids detection process nor yielding normalized noise mask. As mentioned earlier, if some parts of an iris are out of framework, detected outer boundary will not be a complete circle. We are, therefore, able to save the locations of lost pixels in the noise mask during the iris normalization. Among all introduced noise factors in the first section only eyelid has regular shape by and large, a parabola. Consequently, one can detect the eyelids using parabolic Hough transform. The eyelash occlusion makes the eyelid detection inefficient. Hence, we apply 1D rank filter in the horizontal direction before edge extraction and then using the Canny edge detector in the vertical direction the edges are extracted. By this way, the effect of eyelash occlusion is minimized. The parabolic Hough transform including rotation factor to consider head tilt of users is as follow.

$$(\sin\theta(x-h)+\cos\theta(y-k))^2-a(\cos\theta(x-h)-\sin\theta(y-k))=0 \quad (1)$$

Where (h, k) is the vertex point of the parabola, a is the curvature and θ denotes rotation angle. Eye rotation is changed to horizontal shift in the normalized iris image. This gives an opportunity to get rid of rotation term in the above equation by supposing θ equals to 90°as:

$$(x-h)^2+a(y-k)=0 \quad (2)$$

After parabola parameters are found, no eyelid occlusion would be considered if the count of points to construct the parabola is very more than the count of edge pixels contributing in vote-gathering of Hough transform. This often takes place due to very complex textures in some irises. Finally, the locations of right detected eyelids are added to noise mask.

By removing the eyelids from iris region, the other artifacts can be grouped as following: The ones have higher intensity than iris pixels (reflections and sclera) and the ones have lower intensity than iris pixels (eyelashes and pupil). In view of the fact that these noise factors do not show a regular shape, an alternative can be thresholding to detect them. Our aim is to find appropriate threshold(s). The probability of eyelash occlusion in upper iris region is more than the lower part. The observations show that eyelash obstruction in the lower half of the iris is insignificant. Therefore, pupil is only noise factor with low intensity can obstruct the lower half of the iris. The pupil occlusion occurs in few upper rows of normalized iris image. We do not regard the few upper rows (in our experiments 5 rows) in what follows and pupil is separately isolated from iris plane using a threshold that is calculated based on localized pupil in the previous section. Consequently, only high intensity noise factors can obstruct the rest of the lower part of the iris. Finding the optimal threshold(s) to detect the other noise factors is difficult because of variations in the environmental conditions and changing the intensity of them even for two images from the same subject. A novel algorithm is proposed in this paper, namely statistical decision making (SDM) to check this hypothesis that whether there is occlusion and if it is proved, the threshold(s) will be calculated. One of the key parameters in this algorithm is skewness, which is a statistical parameter to measure the asymmetry of a distribution and defined as:

$$\gamma=\frac{E\left\{(x-\mu)^3\right\}}{\sigma^3} \quad (3)$$

$E\{x^3\}$ is the third moment about the mean μ and σ is a standard deviation. The positive skewness value indicates the right tail is longer while the negative skewness value indicates the left tail is longer. For more comprehension, the flow chart of the proposed method (SDM) is illustrated in Figure 3. The following steps explain the details of the proposed method.

- If each half of the iris region is severely obstructed by high intensity noise factors, the skewness value will be positive and significant as the below condition is satisfied

  $$\gamma > k_1 \quad (4)$$

  k_1 is a positive constant. When occlusion hypothesis is proved the appropriate threshold will be calculated by the following equation for each occluded part.

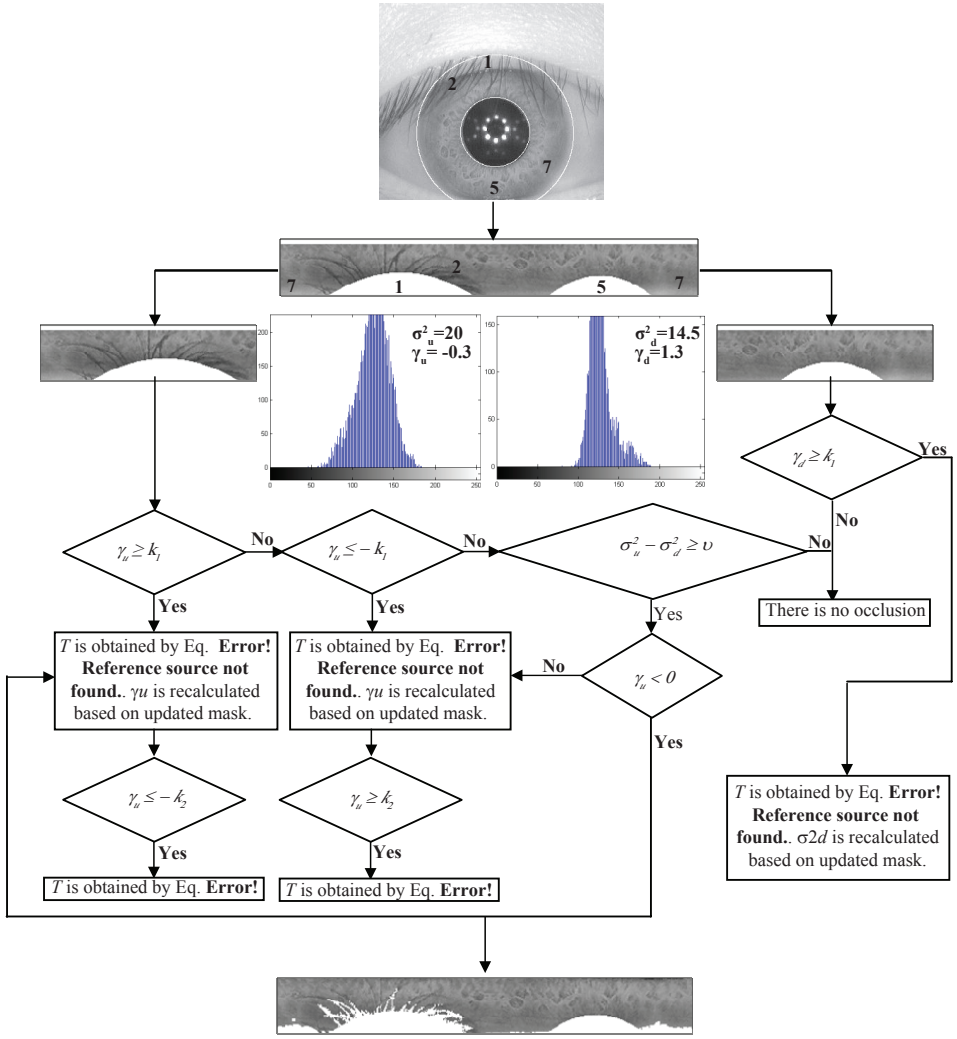

Figure 3: Finding appropriate threshold(s) by SDM to detect the eyelashes, reflections and sclera

$$T = \frac{\sum_{i=G+1}^{255} h_i \times i}{\sum_{i=G+1}^{255} h_i} - \beta \qquad \gamma(0-G) \to 0^- \qquad (5)$$

Where i is gray level of a 8-bit image, h_i denotes histogram counts of unmasked pixels of each half of the iris, G is a gray level that distribution of the pixels with equal or lower intensity than it has negative skewness value and β is a positive constant to bias the optimal threshold T. Locations of the pixels with gray level higher than T are added to noise mask

- Due to pupil occlusion is separately detected; the eyelashes are only low intensity noise factor in the upper half of the iris. In the case of eyelash occlusion, the skewness value will be negative and significant as the below condition is satisfied

$$\gamma < -k_1 \qquad (6)$$

When eyelash occlusion hypothesis is proved the appropriate threshold will be calculated by the following equation

$$T = \frac{\sum_{i=0}^{G-1} h_i \times i}{\sum_{i=0}^{G-1} h_i} + \beta \qquad \gamma(G-255) \to 0^+ \qquad (7)$$

In Eq. 7 G is a gray level that distribution of the pixels with equal or higher intensity than it has the positive skewness value. Locations of the pixels in the upper half of the iris with gray intensity lower than T are added to noise mask

- If the upper half of the iris is obstructed at once by both high and low intensity noise factors, the skewness value will be close to zero. In this case, gray intensity variance of the upper half of the iris is larger than the lower one. The gray intensity variance is calculated for noise-free

pixels. Therefore, occlusion hypothesis will be accepted if the following condition is established.

$$\sigma_u^2 - \sigma_l^2 > \upsilon \quad (8)$$

Where σ_u^2 and σ_l^2 represent the gray intensity variance of upper and lower half of the iris, respectively. v is a positive constant. In this case, for positive value of the skewness pertaining upper iris part, if Eq. 4 is satisfied for k_2 instead of k_1 (i.e., $k_2 < k_1$) the hypothesis of occlusion by high intensity noise factors are accepted and the appropriate threshold is calculated by Eq. 5. Also, for negative skewness value of upper iris part, if Eq. 6 is satisfied for k_2 instead of k_1 (i.e., $k_2 < k_1$) the eyelash occlusion hypothesis is accepted and the appropriate threshold is calculated by Eq. 7. After that, the noise mask is updated based on detected noisy pixels. Then, the skewness value is recalculated for unmasked pixels and if its sign is changed compared to before updating noise mask and Eq. 4 (or 6) is satisfied for k_2 instead of k_1 the appropriate threshold is obtained by Eq. 5 (or 7) for the other noise factors. Similarly, this methodology is done for last two steps to detect the other noise factors with partial occlusion.

As mentioned earlier, the intensity of each eyelash changes a little along the eyelash. Hence, using the thresholding may not afford to detect the entire of eyelash. To obviate this inconvenience, we use an iterative algorithm similar to Kong's and Zhang's idea[9] that was proposed to detect the weak reflections close to strong reflections. The unmasked pixels which connected to any eyelash pixel are checked by the following statistical test.

$$I(x, y) < \mu - \alpha\sigma \quad (9)$$

Where I (x, y) is gray intensity of the unmasked pixels, which connected to any eyelash pixel, μ and σ are gray scale mean and standard deviation of unmasked pixels in upper iris part and α is a positive constant to control the detection of intensity changes along an eyelash. If inequality (9) is satisfied, the noise mask will be updated by adding the location of pixel (x, y) as eyelash. After testing all neighbor pixels of eyelash pixels by Eq. 9 the value of μ and σ are recalculated based on updated noise mask and this is repeated until no neighbor pixels support Eq. 9. The intensity of some iris stripes is close to eyelash intensity. Therefore, some of them may be considered as eyelashes by thresholding. A connective criterion checks the connectivity of each eyelash pixel to other eyelash pixels or to eyelid pixels. The eyelash pixels, which not be able to satisfy this criterion will be removed from the noise mask as iris textures.

SDM globally calculates the statistical measurements to find appropriate threshold(s) while most of the state-of-the-art algorithms such as developed systems in[9,12,13] used local statistical measurements to get their parameter as it puts complexity on the system. Furthermore, in[2] Daugman indicated to use differences between intensity distribution of different parts of iris for calculation of appropriate threshold without providing any details. Tan *et al*.[10] used an idea like Daugman to obtain optimal threshold, which is involved in the training stage. One of the advantages of SDM is the capability to find three thresholds (one for eyelashes and two for reflections of upper and lower parts of the iris) while Daugman's and Tan's systems can be found only one threshold to detect the eyelashes. Two separate thresholds are considered for reflections of upper and lower parts of the iris because our observations show that the intensity gray of reflections in them may be different.

SHAPE ADAPTIVE IRIS FEATURE EXTRACTION

Iris has rich textures so that it provides significant discrimination between subjects. Iris representation is one of the substantial steps in the iris recognition as the system performance depends on it directly. In the matching step, the noisy features are not compared using the information provided by noise mask about obstructed areas. However, we cannot ensure that the noisy parts do not participate in the extraction of clean features. Once a feature represents the information in an image region which contains little noisy data, it may be participated in the matching as clean feature but it is affected by noisy data. This situation happened for a group of patterns including the boundary between noisy and noise-free data. This section describes how the shape adaptive robust features are extracted using two approaches and based on the noise mask.

Shape Adaptive Wavelet Transform Feature Extraction

SAWT is used in the object-based image coding. In this technique, a binary shape mask is used to define the region of interest (ROI) for coding. The image and corresponding shape mask are decomposed into some sub-bands in the same way as the discrete wavelet transform (DWT) works. However, the coefficients are only derived from the image pixels of ROI. This approach can be exploited in our application using the noise mask to determine the iris region as ROI. Figure 4 shows one level of decomposition of a normalized iris image by SAWT. The LL sub-band is used for the next level of decomposition. The iris codes are generated by an encoding strategy based on the sign of each coefficient of LH and HL sub-bands in the fourth level of decomposed image. In addition, the mask codes are generated by the bits of LH and HL sub-bands in the fourth level of pertaining decomposed mask to assign the noisy bits in the iris codes. Comparably, we also generate the iris codes by DWT coefficients same as SAWT feature extraction to evaluate the effect of shape adaptive idea on the system performance. A 2D down-sampling is applied to the noise mask for binary decomposition. Figure 5 shows two levels

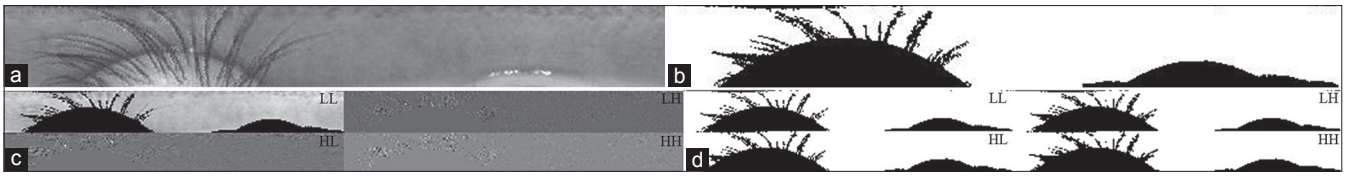

Figure 4: One level of decomposition of an iris image by SAWT. (a) Original image, (b) Noise mask, (c) Decomposed iris image, (d) Decomposed noise mask

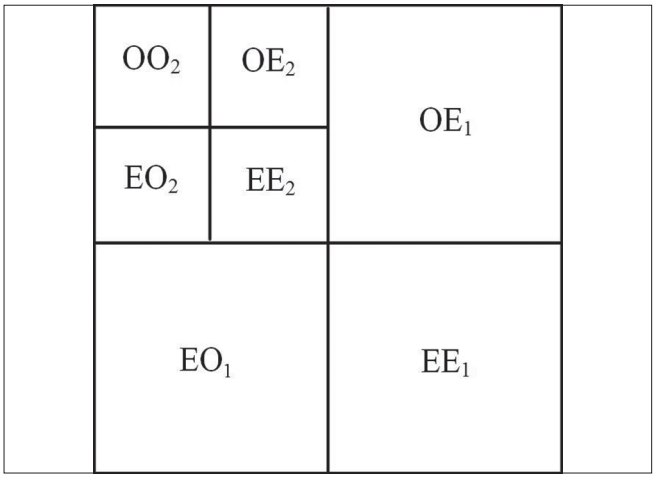

Figure 5: Two levels of 2D down-sampling

of 2D down-sampling. 'O' and 'E' stand for sampling of odd and even columns or rows, respectively. For DWT feature extraction, the mask codes are generated by the bits of OE and EO sub-bands in the fourth level of decomposed mask by 2D down-sampling.

Shape Adaptive Gabor-Wavelet Feature Extraction

Gabor-Wavelet can represent the iris patterns effectively by decomposing the image in more directions. In our earlier work[6] a novel Gabor parameter selection has been proposed and the Gabor parameters values have been optimized using multi objective genetic algorithm. The right upper quarter of normalized iris image was used for feature extraction in order to omit the noise-removing step in our earlier work. However, in this paper, our optimized Gabor-wavelet is used to extract the features from whole normalized image using the reported values in.[6] The iris codes are obtained by extending the novel iris encoding strategy, namely Amplitude Texture Variations which was proposed in,[6] to whole normalized iris image as follows.

$$c_{p,q} = \begin{Bmatrix} 1, if \left|H_{p,q+\lambda}(x_0, y_0)\right| > \left|H_{p,q}(x_0, y_0)\right| \\ 0, otherwise \end{Bmatrix} \quad (10)$$

Iris code C is obtained for $P = 1,2,\ldots, P$ and $q = 1,2\ldots, Q$; where P and Q are the number of the image blocks in the vertical and horizontal direction in the normalized iris image, respectively. λ is a positive constant which controls the comparison length. Once the image capturing unit is would not be efficient, λ is chosen large enough to limit the effects of the blurred images on the performance. On the contrary, λ would have small value for systems that have effective image acquisition system. For $q = Q - \lambda + 1, Q - \lambda + 2,\ldots, Q$ the above equation is run periodically. $H_{p,q}(x_0, y_0)$ is complex coefficient of filtered image by Gabor-Wavelet and $|\cdot|$ stands the amplitude. The reason of dividing the normalized iris image to several image blocks is to decrease the redundancy. Similarly, the noise mask is divided into several blocks and each block is tested by the following two-fold function to determine whether the corresponding bit in iris code is noisy or not.

$$m_{p,q} = \begin{Bmatrix} 1, if\ L_{p,q}(x_0, y_0) > k \times \sum_{i=1}^{n}\sum_{j=1}^{n}\left|G(i,j)\right| \\ 0, otherwise \end{Bmatrix} \quad (11)$$

Where $G(i, j)$ is a Gabor filter with size $n \times n$ and k has a value in (0,1). $L_{p,q}(x_0, y_0)$ is defined as:

$$L_{p,q}(x_0, y_0) = N_{p,q}(x_0, y_0) * |G(x_0, y_0)| = \sum_{i=1}^{n}\sum_{j=1}^{n} N_{p,q}(i, j).|G(i, j)| \quad (12)$$

In this equation, $N_{p,q}(x_0, y_0)$ indicates the block at the p^{th} row and q^{th} column of the noise mask and (x_0, y_0) is taken as the center of each block. Since the energy of a Gabor filter is centralized, the position of the noise is paid attention in Eq. 11.

To extend the shape adaptive approach to Gabor-Wavelet, it needs to study the principles of SAWT in some details. 2D separable wavelet decomposition is carried out in horizontal and vertical directions separately and each segment of rows or columns of ROI is decomposed by wavelet filter in SAWT. One of the issues in SAWT is how to deal with wavelet transform for arbitrary length image segment.[15] To have the perfect reconstruction condition for the wavelet transform, the lost pixels should be filled with the values of the pixels inside the image segment. This is called boundary extension for applying the wavelet filters to the borders of image segments based on the number of taps for each filter. The extensions include periodic extension and symmetric extensions (see Li and Li[15] for more details). In this way, the lost pixels are filled with nearest valid pixel in the same row or column though it may not be nearest neighbor. In other words, the separable SAWT cannot always find the nearest neighbor, which it may be in the other rows or columns. However, non-separability of Gabor-wavelet provides an opportunity to find the nearest neighbor more effectively. Therefore, for having shape adaptive Gabor-wavelet, we

fill the noisy pixels in each acceptable block from view of Eq. 11 by nearest neighbor pixel in the same block. Then, the Gabor-wavelet is applied to enhanced image block and iris codes are obtained by using Eq. 10.

The iris codes are compared by hamming distance (HD) as defined below:

$$HD = \frac{\left\|(C_1 \otimes C_2) \cap M_1 \cap M_2\right\|}{\left\|M_1 \cap M_2\right\|} \quad (13)$$

Where C_i and M_i are iris code and mask code, respectively. $\otimes$ and $\cap$ are logical operators XOR and AND, respectively.

EXPERIMENTAL RESULTS

The proposed scheme is evaluated in this section. The images from CASIA-IrisV3-Interval database[16] and UBIRIS V1 database[17] are used to test the proposed scheme. CASIA-IrisV3-Interval database includes 2655 iris images from 396 different classes of 249 subjects. The iris samples were captured under NIR lighting. Each 8-bit gray-scale iris image is stored as JPG with resolution of 320 × 280 pixels. UBIRIS V1 database includes 1877 iris images, which were collected under VL lighting in two sessions. First session contains 1214 images from 241 individuals while in the second session; only 132 individuals have been participated to capture 663 images. The 24-bit RGB color iris images are stored as JPG with resolution of 800 × 600 pixels. We convert them to gray scale images with resolution of 400 × 300 pixels. We prefer to use these databases because they contain many noisy iris images due to occlusions by eyelids, eyelashes and reflections. Some iris images of UBIRIS V1 database do not have meaningful information due to hard occlusion or bad lighting. On the other hand, each iris classes should have at least four images, three for enrollment and others for recognition. Thus, only 2578 iris images from 353 classes for CASIA-IrisV3-Interval database and 1751 iris images (1183 images from 237 classes for the first session and 568 images from 116 classes for second session) can be used in our experiments. Figure 6 shows some localized iris images from these two databases. The localized iris region is transformed to a normalized rectangular image with size 64 × 512 using Daugman rubber sheet model.[1] The values of SDM parameters are: $\beta = 15$, $v = 2$, $\alpha = 2$, $k_1 = 0.5$, $k_2 = 0.2$ for CASIA andfor UBIRIS. As can be seen, the SDM parameters are almost same for both databases and in turn, SDM is compatible with any database. Figure 7 illustrates visual effect of proposed noise-removing approach on the normalized iris images. For the iris images from UBIRIS database, the shadows by eyelashes due to VL capturing cause hard to detect the eyelashes. However, as can be seen in Figure 7, the proposed noise-removing approach copes to detect them effectively. Biometric

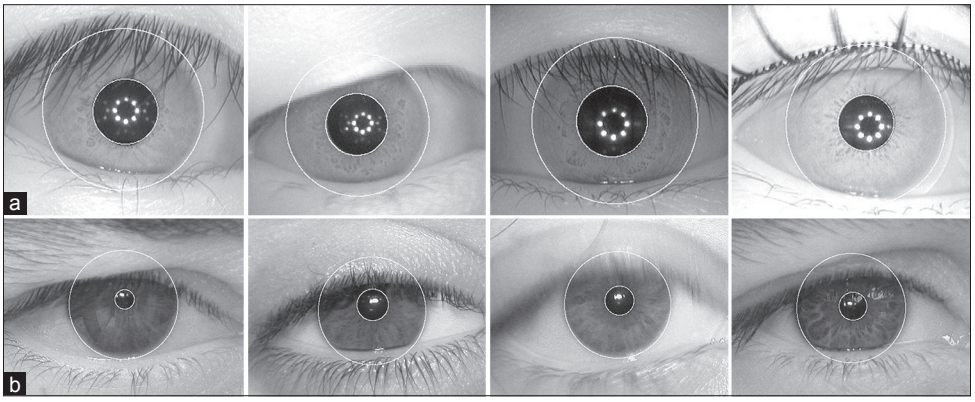

Figure 6: Some localization results for samples from (a) CASIA database, (b) UBIRIS database

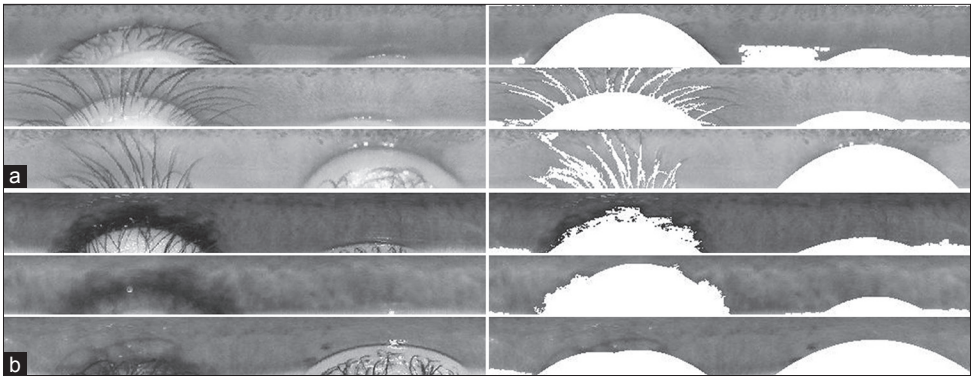

Figure 7: Visual effect illustrations of proposed noise-removing approach. Left column shows before applying noise-removing and right column shows after applying noise-removing. (a) CASIA database, (b) UBIRIS database

systems work in two modes: Identification (e.g., one-to-all) and verification (e.g., one-to-one). Correct recognition rate (CRR) is used to test the identification mode as the ratio of the number of correct classifications to the total test samples. The performance of the verification mode is evaluated by equal error rate (EER), which is the error percentage that False Accept Rate (FAR) equals to False Reject Rate (FRR). We use 9/7 filter for SAWT feature extraction. Furthermore, 9/7 filter is used to extract the features by DWT to evaluate the effect of shape adaptive idea on the system performance. The iris codes are generated using the information of LH and HL sub-bands in the fourth level and therefore, the length of iris codes and mask codes is 256 bits. The Gabor filter bank which is used here has four filters that the Gabor parameters selection is done by reported values in our earlier work.[6] The size of the image blocks and Gabor filters is 9×9 (i.e., $n = 9$) as $P = 8$ and $Q = 64$. Therefore, the iris codes and mask codes contain 2048 bits. The parameter of λ in Eq. 10 is chosen 1 and 3 for the images of CASIA and UBIRIR database, respectively. We consider larger value for λ in the images of UBIRIS database because some images are blurred due to moving or bad focusing especially in the second session. The k parameter in Eq. 11 has a compromising role between noise-removing and number of bits that are actually available for comparison. Large values for k produce more reduction in the number of effective bits to be compared. The reliability of the obtained results is enhanced by more participated bits in the matching step. The effect of various values of k on EER and CRR for both databases is demonstrated in Figure 8. The performance comparisons for wavelet transform and Gabor-Wavelet feature extraction including with and without shape adaptive are provided in Table 1. In addition, to evaluate the performance improvement by proposed noise-removing approach, we present a system without noise-removing step (i.e., without a mask in Eq. 13 in this table. Receiver Operating Characteristic (ROC) curve plots FRR against FAR. The recognition accuracy is compared by ROC curves in Figure 9. The value of k is considered 0.7 for the systems which are presented in Figure 9 and Table 1.

By evaluating the obtained results we can list the following conclusions:

- Using shape adaptive transforms for iris feature extraction does not make a significant improvement while it imposes complexity on the system especially for shape adaptive Gabor-Wavelet due to multi directional boundary extension. In some cases, the performance of SAWT feature extraction reduces relative to DWT feature extraction (without shape adaptive). This comes from the boundary extension in SAWT, which is done in one direction, horizontal or vertical
- Gabor-wavelet decomposes the textures in more directions (four directions here) while the wavelet transform decomposes the textures only in vertical and horizontal directions. Hence, Gabor-wavelet feature extraction produces more distinction. Moreover, one can optimize the Gabor parameters to reach best accuracy while this is not possible in wavelet feature extraction. In addition, proposed encoding for extracted features by Gabor-Wavelet is compatible with iris texture variations as it causes to decrease the recognition error

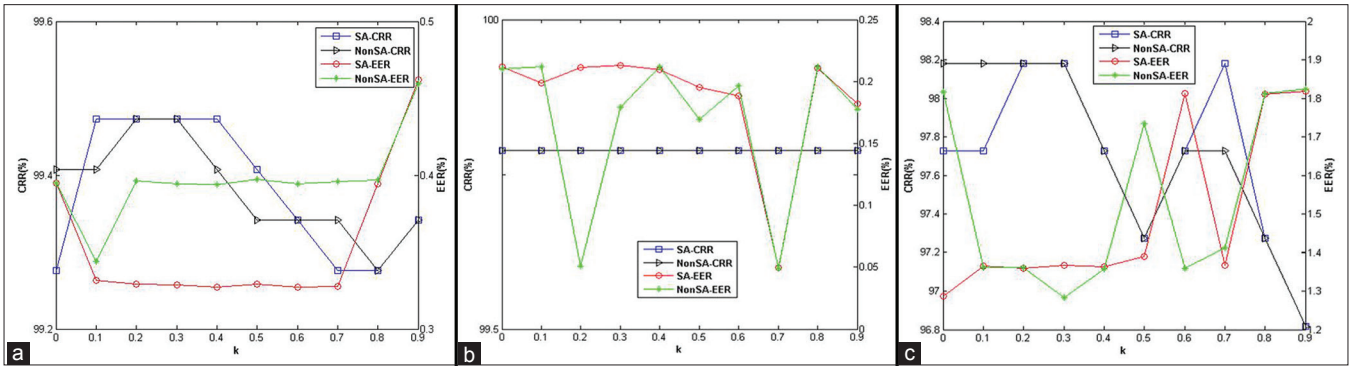

Figure 8: Comparison equal error rate and correct recognition rate results for various values of k. (a) CASIA, (b) UBIRIS session I, (c) UBIRIS session II

Table 1: Recognition accuracy comparisons

Method	CASIA		UBIRIS (session I)		UBIRIS (session II)	
	CRR (%)	EER (%)	CRR (%)	EER (%)	CRR (%)	EER (%)
Without mask-Gabor	98.49	0.85	99.58	0.42	97.27	2.27
Without mask-DWT	95.72	2.88	99.36	0.64	95.45	3.73
Gabor	99.41	0.39	99.79	0.05	97.73	1.41
SA Gabor	99.50	0.33	99.79	0.05	98.18	1.37
DWT	97.30	1.84	99.79	0.42	95.91	4.09
SAWT	97.24	1.63	99.58	0.43	95.91	4.43

DWT – Discrete wavelet transform; SAWT – Shape adaptive wavelet transform; CRR – Correct recognition rate; EER – Equal error rate; UBIRIS – University of beira interior iris database; CASIA – Chinese academy of sciences institute of automation

- Due to extracting the features from high level sub-bands of decomposed iris textures by wavelet transform, the length of iris codes is short. However, this is not considered as an advantage. In fact, we observed using the information of low level sub-bands to generate the iris codes decreases the system performance because of accompanying noise with high frequency components. Therefore, to reduce the influence of noise on the results, low frequency sub-bands are used to generate the iris codes.
- Using low signature size in noisy environments produces decrease in recognition accuracy. Furthermore, the advantages of using masks disappear when the iris code length is short. This is the reason of degradation in recognition rate for wavelet features including masks against a system without masks for second session of UBIRIS database, which is captured in very noisy environment.
- An effective feature extraction algorithm should be robust against segmentation errors. The accuracy of our localization method on CASIA database is less than on UBIRIS database. This is why that the recognition rate of extracted features by wavelet transform degrades more than Gabor features on CASIA database. This shows that the robustness of wavelet feature extraction is less than Gabor-wavelet feature extraction.

In order to compare the proposed scheme with existing methods, we try to find the state-of-the-art approaches that were implemented using the iris databases employed in this paper. These results are presented in Tables 2 and 3 for CASIA-IrisV3-Interval and UBIRIS v1 databases, respectively. We rarely find the papers, which were considered both aforementioned databases. Therefore, separate tables are provided for each database. Sun and Tan[18] used multilobe differential filters for ordinal iris feature extraction. The best performance is for combining the di-lobe and tri-lobe for nonlocal ordinal codes, which is brought in Table 2. Tsai *et al*.[19] proposed fuzzy grayscale curve tracing to segment the iris region. Then, they used a filter bank including 12 Gabor filters corresponding to two frequencies and six orientations to extract 96 local real-valued feature points. The matching strategy was based on fuzzy clustering algorithm. Their system was tested for identification and verification mode, which the results can be seen in Table 2. Masek[3] detected the eyelids using linear Hough transform and the eyelashes using a constant threshold. Ma *et al*.[20] used 1D quadratic spline wavelet to address the position of local sharp variation points in the normalized iris image as the features. Rathgeb *et al*.[21] exploited the previous approaches for feature extracting and adopted selective bits fusion to pick out the distinctive bits. In Table 2, we use the reported values for Masek's and Ma's method by Rathgeb *et al*.[21] through re-implementing these methods. Tajbakhsh *et al*.[5] extracted the robust features from lower half of the iris based on local intensity variations. For each iris image, they generated five iris codes and then used

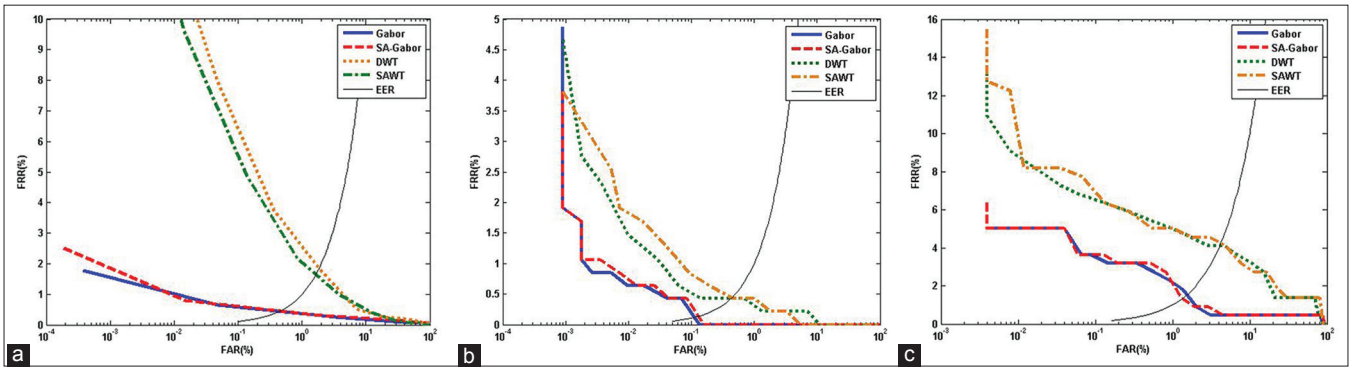

Figure 9: Receiver operating characteristic curves for wavelet transform and Gabor-Wavelet feature extraction including with and without shape adaptive and noise-removing on the database. (a) CASIA. (b) UBIRIS session I. (c) UBIRIS session II

Table 2: Performance comparisons using CASIA database

Method	CRR (%)	EER (%)	Feature length	Feature extraction running time (ms)	Number of tested images
Sun and Tan[18]	-	0.35	2048 bits	10.4	Not determined
Tsai *et al*.[19]	99.97	0.40	96 real-valued features	Not determined	2553
Masek[3]*	-	1.41	10240 bits	Not determined	1332
Ma *et al*.[20]*	-	1.83	10240 bits	244.2	1332
Rathgeb *et al*.[21]	-	1.15	6336 bits	Not determined	1332
Proposed method (Gabor)	99.41	0.39	2048 bits	285.6	2578
Proposed method (SA Gabor)	99.50	0.33	2048 bits	533.2	2578
Proposed method (DWT)	97.30	1.84	256 bits	112.5	2578
Proposed method (SAWT)	97.24	1.63	256 bits	140.7	2578

*The experimental results are reported in[21] by re-implementing these methods. CRR – Correct recognition rate; EER – Equal error rate; DWT – Discrete wavelet transform; SAWT – Shape adaptive wavelet transform; CASIA – Chinese academy of sciences institute of automation

Table 3: Performance comparisons using UBIRIS database

Method	CRR (%)		EER (%)		Feature length	Feature extraction running time (ms)	Number of tested images
	First session	Second session	First session	Second session			
Poursaberi and Araabi[22]*	-	-	2.10	5.00	544 bits	Not determined	1740
Ma *et al*.[20]*	-	-	1.90	5.00	5280 bits	244.2	1740
Monro *et al*.[23]*	-	-	1.20	3.80	2343 bits	30	1740
Tajbakhsh *et al*.[5]	-	-	0.40	3.00	5×256 bits**	Not determined	1740
Pinheiro *et al*.[24]	97.44	96.33	3.39	5.83	18400 real-valued features	Not determined	Not determined
Chen *et al*.[25]	-	-	0.35	-	1536 bits	Not determined	975
Proposed method (Gabor)	99.79	97.73	0.05	1.41	2048 bits	291.1	1751
Proposed method (SA Gabor)	99.79	98.18	0.05	1.37	2048 bits	549.8	1751
Proposed method (DWT)	99.79	95.91	0.42	4.09	256 bits	120.2	1751
Proposed method (SAWT)	99.58	95.91	0.43	4.43	256 bits	147.3	1751

*The experimental results are reported in [5] by re-implementing these methods; **The authors of [5] generated five iris codes for each iris image and used SVM-based fusion rule to make the decision. CRR – Correct recognition rate; EER – Equal error rate; DWT – Discrete wavelet transform; SAWT – Shape adaptive wavelet transform; UBIRIS – University of beira interior iris database

SVM-based fusion rule for decision making. In addition, they re-implemented the works in[20,22,23] on the UBIRIS database, which the results are reported in Table 3. Pinheiro *et al*.[24] used Novelty filter to extract the real-valued features. Chen *et al*.[25] extended the idea of feature extraction using 2D gray level co-occurrence matrix to 3D one to obtain the edge information from four orientations. Their system was only tested on the first session of the UBIRIS database and the results are listed in Table 3. These numerical evaluations show the proposed method for Gabor-Wavelet feature extraction provides a significant improvement on the recognition rate especially for UBIRIS database while we use more images than the others. Using the accurate localization algorithms such as active contours and level set, it can make more improvements on the performance and we will concentrate on this step in our future endeavors.

CONCLUSION

In this paper, we investigated the effect of shape adaptive transforms to exclude the noisy pixels in feature extraction step. In this way, SAWT and shape adaptive Gabor-Wavelet are used to extract the features. Experimental results demonstrate the shape adaptive transform cannot make a significant improvement on the recognition rate. However, the proposed scheme achieves the best performance among state-of-the-art approaches while it is tested by more images than the others from the CASIA-IrisV3-Interval database and UBIRIS V1 database. This owes to the novel noise-removing approach proposed in this paper. It effectively detects eyelids, eyelashes, reflections, out of framework, pupil and sclera as noise factors in the normalized iris images. The novelty is to detect eyelashes and reflections through finding appropriate thresholds by a procedure called SDM. In addition, an accurate and fast iris localization approach based on coarse-to-fine strategy is presented. Furthermore, we elaborate how the mask codes are generated to exclude the noisy bits in an iris code. Literature reviews show there are not any details about the mask code generation.

ACKNOWLEDGEMENT

We highly appreciate Iran Research Centre of Intelligent Signal Processing (RCISP) for its support to this research as a part of M.Sc thesis.

REFERENCES

1. Daugman JG. How iris recognition works. IEEE Trans Circuits Syst Video Technol 2004;14:21-30.
2. Daugman J. New methods in iris recognition. IEEE Trans Syst Man Cybern B Cybern 2007;37:1167-75.
3. Masek L. Recognition of human iris patterns for biometric identification. Bachelor Thesis, University of Western Australia, 2003. Available from: http://people.csse.uwa.edu.au/pk/studentprojects/libor.
4. Miyazawa K, Ito K, Aoki T, Kobayashi K, Nakajima H. An effective approach for iris recognition using phase-based image matching. IEEE Trans Pattern Anal Mach Intell 2008;30:1741-56.
5. Tajbakhsh N, Araabi BN, Soltanian-Zadeh H. Noisy iris verification: A modified version of local intensity variation method. International Conference on Advances in Biometrics. Lecture Notes in Computer Science 5558;2009; p. 1150-9.
6. Ghodrati H, Dehghani MJ, Danyali H. Two approached based on genetic algorithm to generate short iris codes. Int J Intell Syst Appl 2012;4:62-79.
7. Qichuan T, Xirong L, Ziliang L, Linsheng L. Imperfect iris information for identity recognition. International Congress on Image and Signal Processing, 2009.
8. Chen Y, Adjouadi M, Han C, Wang J, Barreto A, Rishe N, *et al*. A highly accurate and computationally efficient approach for unconstrained iris segmentation. Image Vis Comput 2010;28:261-9.
9. Kong WK, Zhang D. Accurate iris segmentation based on novel reflection and eyelash detection model. International Symposium on Intelligent Multimedia, Video and Speech Processing, 2001.
10. Tan T, He Z, Sun Z. Efficient and robust segmentation of noisy iris images for non-cooperative iris recognition. Image Vis Comput 2010;28:223-30.
11. Jang YK, Kang BJ, Park KR. A study on eyelid localization considering image focus for iris recognition. Pattern Recognit Lett 2008;29:1698-704.
12. Kang BJ, Park KR. A robust eyelash detection based on iris focus assessment. Pattern Recognit Lett 2007;28:1630-9.
13. Min TH, Park RH. Eyelid and eyelash detection method in the

normalized iris image using the parabolic Hough model and Otsu's thresholding method. Pattern Recognit Lett 2009;30:1138-43.
14. Otsu N. A threshold selection method from gray-level histogram. IEEE Trans Syst Man Cybern 1979;9:62-6.
15. Li S, Li W. Shape-adaptive discrete wavelet transforms for arbitrarily shaped visual object coding. IEEE Trans Circuits Syst Video Technol 2000;10:725-43.
16. CASIA iris image database. Available from: http://www.idealtest.org/dbDetailForUser.do?id=3.
17. UBIRIS dataset obtained from Department of Computer Science. Portugal: University of Beira Interior; http://iris.di.ubi.pt/ubiris1.html.
18. Sun Z, Tan T. Ordinal measures for iris recognition. IEEE Trans Pattern Anal Mach Intell 2009;31:2211-26.
19. Tsai CC, Lin HY, Taur JS, Tao CW. A new matching approach for local feature based iris recognition systems. IEEE Conference Industrial Electronics and Applications. (ICIEA) 2010. p. 387-92.
20. Ma L, Tan T, Wang Y, Zhang D. Efficient iris recognition by characterizing key local variations. IEEE Trans Image Process 2004;13:739-50.
21. Rathgeb C, Uhl A, Wild P. On combining selective best bits of iris-codes. In: European workshop on Biometrics and ID Management. Lecture Notes in Computer Science 6583; 2011; p. 227-37.
22. Poursaberi A, Araabi BN. Iris recognition for partially occluded images: Methodology and sensitivity analysis. EURASIP J Adv Signal Process 2007.
23. Monro DM, Rakshit S, Zhang D. DCT-based iris recognition. IEEE Trans Pattern Anal Mach Intell 2007;29:586-95.
24. Pinheiro CF, Costa MG, Filho CF. Applying a novelty filter as a matching criterion to iris recognition. International Congress Image and Signal Process. 2010; 5: 2414-8.
25. Chen WS, Huang RH, Hsieh L. Iris recognition using 3D co-occurrence matrix. International Conference on Advances in Biometrics. Lecture Notes in Computer Science 5558; 2009; p. 1122-31.

How to cite this article: Ghodrati H, Dehghani MJ, Danyali H. Shape Adaptive, Robust Iris Feature Extraction from Noisy Iris Images. J Med Sign Sens 2012;3:195-244-55.

Source of Support: Nil, **Conflict of Interest:** None declared

BIOGRAPHIES

Hamed Ghodrati recieved the B.S. and M.S. degrees In Electrical Engineering from Azad University of Karaj and Shiraz University of Technology, Shiraz, Iran, in 2006 and 2011. His research interests include biometric especially iris recognition, watermarking, data hiding, image processing and pattern recognition.

E-mail: h.ghodrati@hotmail.com

Mohammad Javad Dehghani received the BS and MS degrees from Isfahan University of Technology, Isfahan, Iran, in 1988 and 1992 respectively, the Ph.D. degree from IIT Madras in 2003, all in communication engineering. In 1993, he joined the faculty of Control Department, School of Electronic Technology, Shiraz University, Shiraz, Iran. Since 2003 he has been on the faculty of the Department of Telecommunication Engineering, Shiraz University of Technology, Shiraz, Iran. His activities have included Image signal processing, digital filter structures, filter banks, wavelet based signal processing and wireless communication. He is a Member of the IEEE.

E-mail: dehghani@sutech.ac.ir

Habibolah Danyali received the B.Sc. and M.Sc. degrees in Electrical Engineering respectively from the Isfahan University of Technology, Isfahan, Iran, in 1991 and the Tarbiat Modarres University, Tehran, Iran, in 1993. From 1994 to 2000 he was with the Department of Electrical Engineering, University of Kurdistan, Sanandaj, Iran, as a lecturer. In 2004 he received his PhD degree in Computer Engineering from the University of Wollongong, Australia. After finishing his PhD he continued his academic work with University of Kurdistan as an assistant professor. As of September 2009, he is with the Department of Telecommunication Engineering, Shiraz University of Technology, Shiraz, Iran. He is a Member of the IEEE. His research interests include data hiding, scalable image and video coding, medical image processing and biometrics

E-mail: danyali@sutech.ac.ir